Inorganic Chemistry
Article
Cite This: Inorg. Chem. XXXX, XXX, XXX−XXX
pubs.acs.org/IC

A CuAAC Click Approach for the Introduction of Bidentate Metal Complexes to a Sulfanilamide-Derived Antibiotic Fragment

Reece G. Miller,[†] Melissa Vázquez-Hernández,[‡] Pascal Prochnow,[‡] Julia E. Bandow,[‡] and Nils Metzler-Nolte*[,†]

[†]Inorganic Chemistry I − Bioinorganic Chemistry, Faculty of Chemistry and Biochemistry, Ruhr University Bochum, Universitaetsstrasse 150, D-44801, Bochum, Germany

[‡]Applied Microbiology, Faculty of Biology and Biotechnology, Ruhr University Bochum, Universitaetsstrasse 150, 44780 Bochum, Germany

Supporting Information

Downloaded by NOTTINGHAM TRENT UNIV at 09:08:26:660 on June 27, 2019
from https://pubs.acs.org/doi/10.1021/acs.inorgchem.9b01186.

ABSTRACT: A simple "click-chemistry" approach was employed in order to functionalize the known antibiotic fragment sulfanilamide with a bidentate pyridyl-triazole pocket, which allowed for the synthesis of ruthenium(II) and rhenium(I) carbonyl chloride complexes. Six new complexes were prepared and comprehensively characterized, including five single crystal X-ray structures, photophysical characterization, and testing for antimicrobial activity. Interestingly, functionalization of the pyridine ring with an *ortho*-hydroxymethyl group resulted in a greater than 100-fold increase in the rate of ligand release in a dimethylsulfoxide solution. Subsequent studies indicated this process could be further accelerated by irradiation with 265 nm light. Structural characterization of four of the complexes indicates that this is the result of a lengthening and weakening of the Re−$N_{Pyridine}$ bond (average ($\mathbf{L^{tri}}$) = 2.19 Å vs $\mathbf{L^{tri}OH}$ = 2.25 Å) due to the steric influence of the hydroxymethyl group. The organometallic rhenium(I) pyridyl-triazole functionality maintains its characteristic fluorescent properties despite the presence of the sulfonamide moiety. Two of the compounds showed modest antimicrobial activity against methicillin-resistant *Staphylococcus aureus*, whereas the structurally similar sulfamethoxazole alone showed no activity under the same conditions.

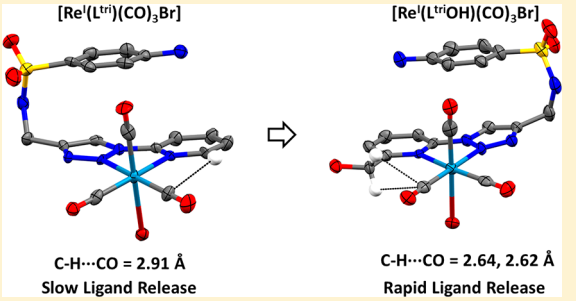

INTRODUCTION

In recent years, the development of new antimicrobial agents has been outpaced by the development of resistance to them.[1] Of particular concern is the spread of methicillin-resistant *Staphylococcus aureus* (MRSA).[1a,b,2] A major problem in drug development is a lack of diversity in modes of action, where some reports suggest that the number of distinct known targets may be limited to 30 or fewer.[3] Because of this, there has been renewed interest in the use of organometallic and inorganic compounds as alternatives to the more commonly used organic antibiotics.[4] Metallodrugs may possess distinct advantages over conventional organic antibiotics including new targets,[4e,f,5] new modes of action,[4e,f,5] which are foreign to the microbes, a greatly increased range of available geometries[4f] (and therefore can fit a greater range of three-dimensional spaces), and targeted activity through light[6] or redox[7] activation.[8] Furthermore, because of their photophysical properties,[9] metallodrugs are also prominent in the emerging field of "theranostics", whereby compounds act as both a therapeutic and diagnostic agent.[4d,10] In many cases, an organic drug fragment and its target are known, and it would be advantageous to be able to easily introduce a metal center in order to improve its biological or physical properties.

The copper(I)-catalyzed azide−alkyne cycloaddition (CuAAC) "click" reaction, originally described independently by the groups of Fokin and Sharpless,[11] as well as Meldal,[12] has found use throughout synthetic chemistry.[13] Examples of this include the synthesis of bioconjugates,[14] dendrimers,[15] and functionalized nanoparticles.[16] Furthermore, the CuAAC click reaction has been used for the synthesis of pyridyl-triazole ligands and metal complexes of them, which have shown promising biological,[17] photophysical,[18] and catalytic properties.[19] More recently, Crowley et al.,[17b,18d] Bertrand et al.,[18a] and Albrecht et al.[20] have extended this approach and investigated the transition metal complexes of bidentate "inverse" (inv) pyridyl-triazole ligands. Here, "inv" refers to pyridyl-triazole ligands, where the metal center is chelated by the pyridine and the central N2 nitrogen atom of the 1,2,3-triazole ring as opposed to the more common N3-pyridine pocket.[18d]

For this proof-of-principle study, the known drug fragment sulfanilamide was chosen. Sulfanilamide belongs to the sulfonamide-class of antibiotics (Figure 1), a well-known drug class, which has been heavily exploited in the treatment of

Received: April 23, 2019

© XXXX American Chemical Society

DOI: 10.1021/acs.inorgchem.9b01186
Inorg. Chem. XXXX, XXX, XXX−XXX

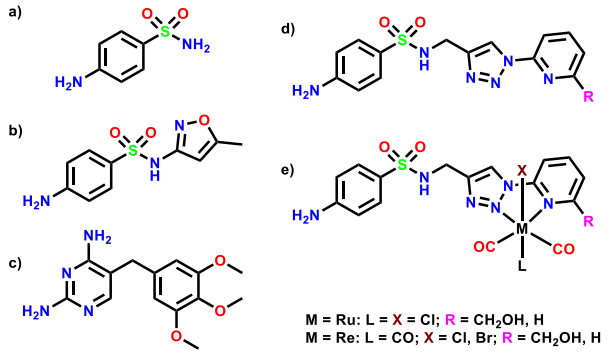

Figure 1. Known organic sulfonamide drugs sulfanilamide (a), sulfamethoxazole (b), folate pathway inhibitor trimethomprim (c), as well as the inv-pyridyl-triazole based ligands (d) and their metal complexes (e) presented in this work.

bacterial infections. Since the discovery of the antimicrobial activity of sulfanilamide, many variations incorporating this drug fragment have been tested. All of these possess the same mode of action: the inhibition of dihydropteroate synthase (DHPS). DHPS is a folate pathway enzyme and is responsible for the synthesis of dihydropteroic acid from *para*-amino-benzoic acid.[21] One of the most commonly used sulfonamide-based antibiotics is sulfamethoxazole (SMX).[22] In practice, SMX is usually used in combination with trimethoprim (TMP) (Figure 1) in a formulation known as cotrimoxazole SMX–TMP.[21−23] The standard formulation is a 1:5 mixture, which results in a 1:20 plasma concentration due to differences in bioavailability.[22] Studies have shown that this 1:20 ratio leads to an optimal cooperative effect.[22] While SMX–TMP is only commonly used in the treatment of urinary tract infections,[24] it has also found use in the treatment of a wide range of bacterial infections from bronchitis and pneumonia[22] to traveler's diarrhea.[25] Furthermore, there has been renewed interest in SMX–TMP for the treatment of methicillin resistant *S. aureus*,[21,26] with the scientific literature indicating good efficacy against some strains of *S. aureus*.[27] However, as with almost all known antibiotics, the use of sulfonamides has been plagued by antibiotic resistance.[21,27a,28] One common mechanism of resistance to sulfonamides is a single amino acid substitution, which weakens the binding of the substrate in DHPS.[27a]

As the binding of sulfonamide antibiotics to dihydropteroate synthase is stabilized by intermolecular hydrogen bonding,[21,29] we hypothesized that the introduction of an organometallic moiety with exchangeable ligands could help to overcome this resistance by introducing a secondary binding interaction—for example, via ligand exchange with a nucleophilic side chain on the protein. Presented herein is a click-chemistry approach for the synthesis of pyridyl-triazole ligands, which have been derived from sulfonamides, and the synthesis of their corresponding rhenium and ruthenium carbonyl complexes.

RESULTS AND DISCUSSION

Synthesis and Structures. The new sulfonamide-based ligands were prepared in two simple steps from commercially available materials (Scheme 1). First, reaction of propargyl bromide with an excess of sulfanilamide allows for preferential alkylation at the more nucleophilic sulfonamide nitrogen. The low yield (17%) was unavoidable due to the activating effect of alkylation, which results in over-alkylation. In order to avoid this, a large excess of sulfanilamide was used, which could then

Scheme 1. Synthetic Route to the New Ligands L^{tri} and $L^{tri}OH$ and their Ru and Re Complexes Reported in This Work[a]

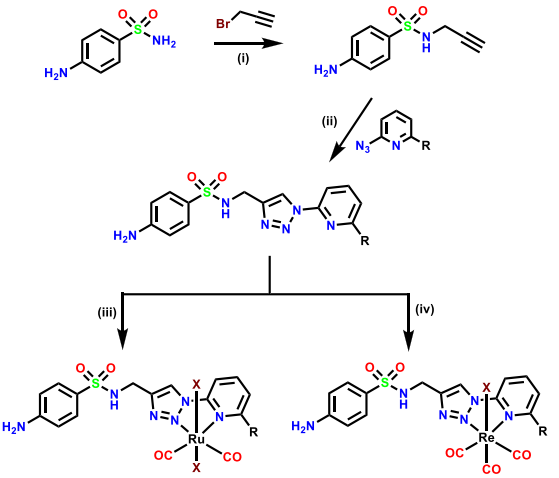

[a]Conditions: (i) K_2CO_3, MeCN, reflux, 4 h. (ii) CuI, Cu(s), NaOAc, DIPEA, toluene/DMF (9:1 v/v), 100 °C, N_2(g). (iii) $[Ru^{II}(CO)_2Cl_2]_n$, EtOH, reflux, N_2(g) (iv) $[Re^{I}(CO)_5Cl]$, EtOH, reflux, N_2(g).

be recovered by column chromatography. The desired pyridyl-triazole ligands can then be obtained in moderate yields (47%) by reaction with the corresponding azido-pyridine using CuAAC "click" chemistry.[17b,18] The corresponding metal complexes could then be obtained in moderate to excellent yields (50%- quantitative) by reaction of the ligands with either $[Ru^{II}(CO)_2Cl_2]_n$ or $[Re^{I}(CO)_5X]$ (Scheme 1). The higher hydrophilicity of $[Ru^{II}(\mathbf{L^{tri}OH})(CO)_2Cl_2]$ relative to the other complexes reduced the recovery of this compound from column chromatography leading to the lower (50%) isolated yield.

Both NMR (Figures S2–S18) and structural (Figures 2–3) evidence confirmed that, despite several potential donor atoms, the only observed products were the desired pyridyl-triazole bound complexes.

Structural Characterization. Four of the metal complexes and one of the ligands were characterized structurally by X-ray crystallography. A summary of the key structural information is given in Table 1. Single crystals of the sulfonamide-ligand $\mathbf{L^{tri}OH}$ were grown from a solution of the ligand in MeCN-d_3, which had been left to slowly evaporate in an NMR tube after characterization by NMR. $\mathbf{L^{tri}OH}$ crystallizes in the monoclinic space group $P2_1/c$ (Figure S25). Adjacent molecules of $\mathbf{L^{tri}OH}$ form strong reciprocated H-bonds between the sulfonamide N–H proton and the OH oxygen atom [N(2)–H···O(3) 2.878(2) Å, 167.8°].

Colorless, needle-shaped crystals of $[Ru^{II}(\mathbf{L^{tri}})(CO)_2Cl_2]$ were grown by vapor diffusion of diethyl ether into a solution of the complex. $[Ru^{II}(\mathbf{L^{tri}})(CO)_2Cl_2]$ (Figure 2, Table 1) crystallizes in the monoclinic space group $P2_1/c$ with one molecule of the complex and one acetone molecule of solvation in the asymmetric unit. The chloride ligands adopt the usual trans arrangement in the axial positions, which has been observed for related complexes such as bipyridyl[30] and pyridyl-1,2,4-triazole based ligands.[31] Therefore, the two carbonyl ligands are cis relative to one another and lie in a square plane with the bidentate ligand. The Ru–N(4)bond is only slightly shorter than that of the Ru–N(6) bond. The

DOI: 10.1021/acs.inorgchem.9b01186
Inorg. Chem. XXXX, XXX, XXX–XXX

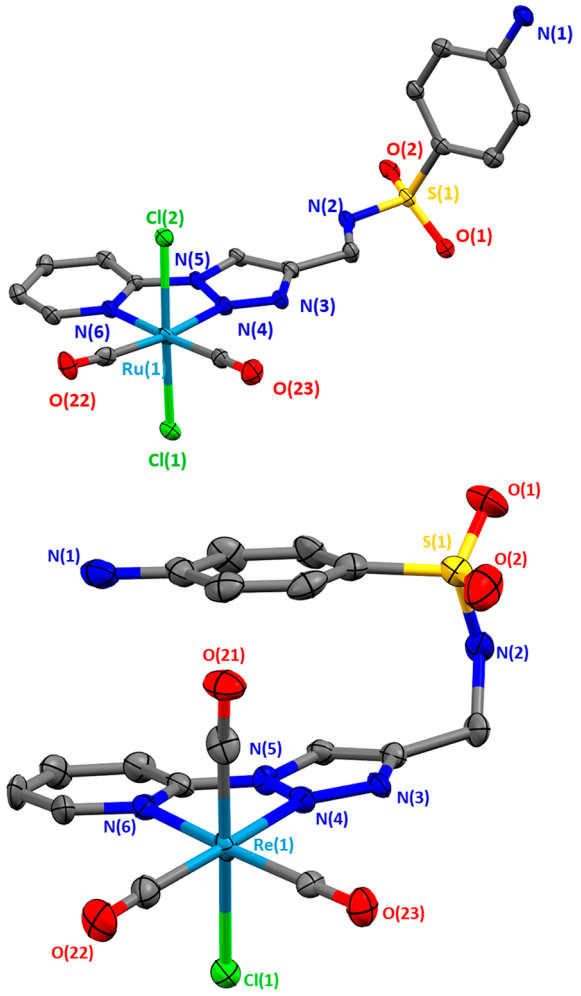

Figure 2. Solid state structures of $[Ru^{II}(\mathbf{Ltri})(CO)_2Cl_2]$ (top) and $[Re^{I}(\mathbf{Ltri})(CO)_3Cl]$ polymorph B (bottom). H atoms and solvent molecules have been omitted for clarity. Thermal ellipsoids are shown at the 50% probability level.

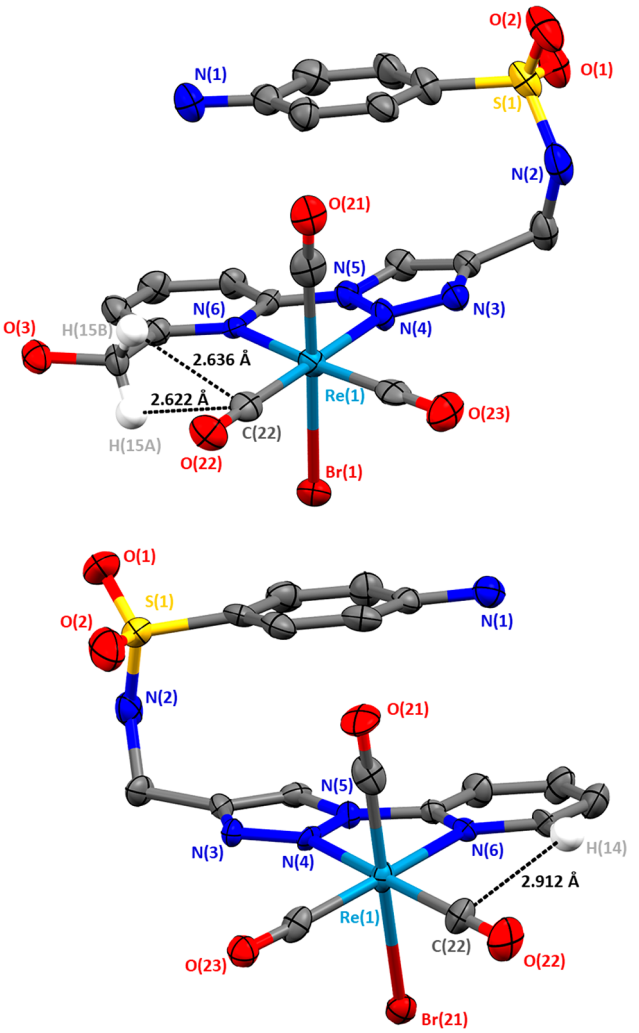

Figure 3. Solid state structures of $[Re^{I}(\mathbf{L^{tri}OH})(CO)_3Br]$ (top) and $[Re^{I}(\mathbf{L^{tri}})(CO)_3Br]$ (bottom). H atoms (except those involved in close H···CO contacts) and solvent molecules have been omitted for clarity. For $[Re^{I}(\mathbf{L^{tri}OH})(CO)_3Br]$, only the major component of the CO/Br disorder is shown. Thermal ellipsoids are shown at the 50% probability level.

acetone molecule of solvation is involved in a strong hydrogen bond to the NH_2 group of the aniline ring [N(1)–H···O(31) 2.948(5) Å, 154.6°].

Highlighter-yellow, plate-shaped crystals of both *rac*-$[Re^{I}(\mathbf{L^{tri}})(CO)_3Cl]$ polymorph B (Figure 2) and *rac*-$[Re^{I}(\mathbf{L^{tri}})(CO)_3Br]$ (Figure 3) were grown by slow evaporation of a solution of the corresponding complex in methanol. The complexes are isostructural and crystallize in the monoclinic space group *Pn* with one stereoisomer in the asymmetric unit and the other being generated by the glide plane.

Therefore, the unit cell comprises both stereoisomers as well as two disordered MeOH molecules. Analogous to the ruthenium complex $[Ru^{II}(\mathbf{L^{tri}})(CO)_2Cl_2]$, the Re–N(4)bonds are slightly shorter than that of the Re–N(6) (Table 1) bond in both complexes. There is however no significant difference in the Re–N and Re–C bond lengths between the two rhenium(I) complexes.

Highlighter-yellow, needle-shaped crystals of *rac*-$[Re^{I}(\mathbf{L^{tri}OH})(CO)_3Br]$ were grown by vapor diffusion of hexane into a solution of the complex in EtOH/acetone (1:1). The complex crystallizes solvent-free in the orthorhombic space group $I4_1/a$ with one stereoisomer in the asymmetric unit and the other being generated by reflection through the glide plane. The main residue is disordered with approximately 12.5% of the molecules having the opposite stereochemistry. Presumably, this occurs because the axial chlorine and carbonyl functionalities can be inverted while only causing minor changes to the crystal packing. Because of the glide plane symmetry, the mixture of isomers within the lattice remains racemic.

In contrast to the complexes of $\mathbf{L^{tri}}$, the Re–N(6) bond is significantly longer than the Re–N(4) bond (Table 1, Figure 3). This lengthening of the Re–N(6) bond can be attributed to the steric influence of the CH_2OH group, whereby short contacts (CH···CO = 2.622 Å, 2.636 Å) between the CH_2 protons and the cis coordinated carbonyl cause the Py–Re bond to be lengthened and weakened. For comparison, the sum of the atomic radii for a H···C contact is 2.8 Å.[32] In contrast, the shortest CH–CO contacts in the rhenium(I) complexes of $\mathbf{L^{tri}}$ fall into the range 2.78–2.95 Å. Furthermore, because of the longer M–Py bond, a slight shortening of the trans M–CO bond is also observed. Moreover, this close contact results in a more distorted octahedron, which is

DOI: 10.1021/acs.inorgchem.9b01186
Inorg. Chem. XXXX, XXX, XXX–XXX

Table 1. Selected Structural Data for the Structurally Characterized Ruthenium(II) and Rhenium(I) Complexes

ML	Re($\mathbf{L}^{tri}$)Br	Re($\mathbf{L}^{tri}$**OH**)Br	Re($\mathbf{L}^{tri}$)Cl (*P*21/*c*) polymorph A	Re($\mathbf{L}^{tri}$)Cl (Pn) polymorph B	Ru($\mathbf{L}^{tri}$)Cl
M−N(6)	2.19(1)	2.245(7)	2.186(6)	2.18(1)	2.135(3)
M−N(4)	2.14(1)	2.132(7)	2.157(6)	2.147(9)	2.103(3)
M−CO eq	1.94(1)	1.88(1)	1.948(9)	1.92(1)	1.892(4)
	1.94(2)	1.92(1)	1.920(8)	1.92(2)	1.892(4)
M−CO ax	1.96(1)	1.92(2)[a,b]	1.89(2)[a,b]	1.94(1)	
CH···CO	2.912	2.622	2.78	2.95	2.74
		2.636			
N(6)−M−N(4)	74.4(4)	73.4(2)	73.9(2)	73.6(4)	76.1(1)
N(6)−M−CO	99.1(6)	105.3(3)	96.4(3)	96.4(5)	95.9(2)
<CO−M−CO	90.2(6)	85.9(3)	88.4(3)	89.8(6)	88.5(2)
N(4)−M−CO	95.7(5)	95.4(3)	91.3(6)	99.9(6)	99.4(2)
O_h distortion[c]	46.5	63.8[a]	58.8[a]	58.3	47.5

[a]Major component of disorder. [b]Although the disorder could be well-modeled, these values should be viewed with caution as the presence of the heavy halogen atom as a minor component of the disorder may interfere with an accurate bond length measurement. [c]Defined as the sum of the deviation of the 12 cis angles from 90°.

reflected in both the octahedral distortion parameter and the larger C(22)−Re−N(6) angle for the substituted complex.

Bright yellow, needle-shaped crystals of [Re^{I}($\mathbf{L}^{tri}$)$(CO)_3$Cl] polymorph A (Figure S26) were grown by vapor diffusion of hexane into a solution of the complex in acetone. The complex crystallizes in the monoclinic space group $P2_1/c$ with one stereoisomer of the complex and one acetone molecule of solvation in the asymmetric unit and the other being generated by glide plane symmetry. Unlike polymorph B, this complex adopts the "extended" conformation (see following paragraph). Here, main residue disorder is again observed with approximately 25% of the molecules having the opposite stereochemistry.

The crystal structures can be divided into two conformational groups: "extended" and "folded". Because of the range of hydrogen bonders and acceptors as well as π-rich and π-deficient ring systems both of these conformers allow for a myriad of inter- and intramolecular interactions. The distinguishing feature of the folded structures is the offset intramolecular $\pi-\pi$ stacking interactions between the aniline ring and the pyridyl-triazole ligand component (Table S3). Conversely, the extended structures are characterized by pairs of reciprocated intermolecular N−H···pi interactions between aniline rings on adjacent molecules, as well as π-stacking interactions between the electron-poor pyridine ring and the electron-rich triazole ring on a further adjacent molecule (Table S4).

Interestingly, in the case of [Re^{I}($\mathbf{L}^{tri}$)$(CO)_3$Cl], different crystallization conditions led to two different polymorphs that represent both the extended and folded conformers of the complex, whereby crystals formed by vapor diffusion of hexane into a solution of the complex in acetone resulted in the extended structure (polymorph A), and crystals grown via slow evaporation of a methanolic solution of the complex adopted the folded structure (polymorph B). Attempts to crystallize the other complexes in both conformers were unsuccessful. This may be due to solubility differences between the two complexes, as the complexes of $\mathbf{L}^{tri}$**OH** are less soluble in neat acetone, and analogous acetone/hexane vapor diffusion experiments resulted in fine powders.

Photophysical Properties. Electronic absorption and emission spectra of all of the complexes were measured in EtOH (Figure 4 and Figure S32).

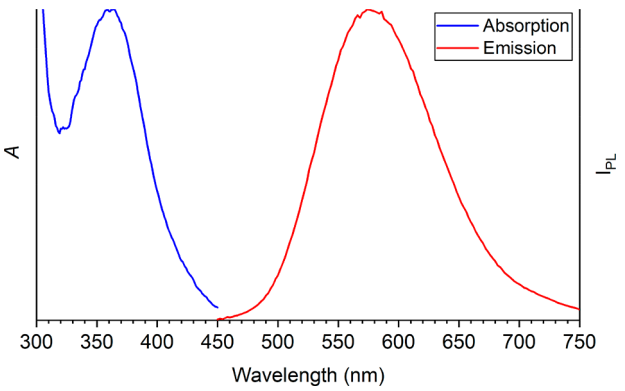

Figure 4. Normalized absorption (A) and photoluminescence (PL) data for a 0.03 mM solution of [Re($\mathbf{L}^{tri}$)$(CO)_3$Cl] in ethanol. The excitation wavelength for PL was 400 nm.

The rhenium(I) complexes show a broad emission band centered around 580 nm (Table 2), which is consistent with

Table 2. Photophysical Properties of the Rhenium(I) and Ruthenium(II) Complexes in Ethanol at 298 K

	absorption	emission	
M	λ_{max} (ε/cm mol^{-1} L^{-1})	λ_{max} (Φ) air	λ_{max} (Φ) N_2(g)
Ru($\mathbf{L}^{tri}$)	265 (27100)		
Re($\mathbf{L}^{tri}$)Cl	265 (29700), 361 (4460)	583 (0.0100)	583 (0.038)
Re($\mathbf{L}^{tri}$)Br	264 (29000), 363 (4350)	583 (0.0095)	578 (0.064)
Ru($\mathbf{L}^{tri}$**OH**)	266 (27600)		
Re($\mathbf{L}^{tri}$**OH**)Cl	265 (29000), 354 (3200)	580 (0.0085)	578 (0.014)
Re($\mathbf{L}^{tri}$**OH**)Br	265 (32000), 357 (3100)	576 (0.0122)	576 (0.024)

related complexes of inv-triazole ligands in the literature.[18a,d] The emission quantum yields were measured in EtOH, both in air and under N_2(g) and are slightly lower than those observed for related compounds measured in DCM or MeCN.[18a,d] These data indicate that the sulfonamide antibiotic fragment has only a minor influence on the photophysical properties of these ligands.

Photochemical Ligand Release. Complexes of ruthenium and rhenium have been shown to undergo photochemical ligand exchange.[8,33] This has generated significant interest for applications such as photoactivated drugs.[8,34]

DOI: 10.1021/acs.inorgchem.9b01186
Inorg. Chem. XXXX, XXX, XXX−XXX

Furthermore, a comparison of "regular" and "inverse" pyridyl-triazole complexes demonstrated photolability for inverse but not regular pyridyl-triazoles.[18a,d] While solutions of the complexes of $\mathbf{L^{tri}OH}$ in coordinating solvents such as dimethylsulfoxide (DMSO) showed significant ligand release after 24 h (up to 35−62%) even when kept in the dark, ligand release was much slower for complexes of $\mathbf{L^{tri}}$, all of which showed minimal (≤5%) release after 48 h. On the basis of NMR integration, the relative rates of ligand exchange between equivalent complexes of each ligand range from ca. 20:1 for $[Re(\mathbf{L})(CO)_3Cl]$ to >100:1 for $[Ru^{II}(\mathbf{L})(CO)_2Cl_2]$ (Figures S36−S40, Table S5).

Furthermore, the complexes of $\mathbf{L^{tri}OH}$ showed slow ligand exchange in MeCN (Figure S41), whereas the complexes of $\mathbf{L^{tri}}$ were stable for up to 2 weeks. Small differences in stability were also observed for the different complexes of each ligand, whereby the fastest rate of ligand exchange was observed for the $[Re(\mathbf{L})(CO)_3Cl]$ complexes.

Solutions of all of the complexes in the coordinating solvent DMSO showed accelerated ligand exchange when visible light was not excluded. For all of the complexes except $[Ru^{II}(\mathbf{L^{tri}})(CO)_2Cl_2]$, the presence of visible light did not result in additional decomposition products. The behavior of $[Ru^{II}(\mathbf{L^{tri}})(CO)_2Cl_2]$ was more complicated with the appearance of at least two other decomposition products in addition to a small amount of free ligand. These decomposition products contained some peaks in the ^{1}H NMR spectrum that could be assigned to the ligand or ligand fragments but did not belong to either the free ligand or the complex $[Ru^{II}(\mathbf{L^{tri}})(CO)_2Cl_2]$. A possible explanation is the substitution of some of the chloride and/or carbonyl ligands with DMSO. However, subsequent analysis by ESI-MS was unable to confirm this.

In order to further investigate the relative rates of ligand photorelease for the rhenium(I) complexes of both ligands, solutions of the complexes in DMSO were exposed to 265 nm light, and the reaction was monitored by UV−vis spectroscopy (Figures 5 and S33). Under these conditions, the ligand loss was further accelerated, whereby complexes of $\mathbf{L^{tri}OH}$ showed complete ligand loss within 4 h (Figure 5 and Figure S32). However, a smaller difference in reaction rates was observed under irradiation, which likely reflects the ability of the complexes of $\mathbf{L^{tri}OH}$ to undergo ligand exchange by a light-independent mechanism. Because of the shorter time scales involved in this experiment, this light-independent ligand loss is less important here.

The accelerated ligand exchange could be due to either electronic or steric effects. As the CH_2OH group is only very weakly inductively electron donating and isolated from mesomeric effects, both the σ-donor and π-acceptor properties of the pyridine ring should be largely unaffected. Therefore, electronic effects are only expected to play a minor role in the stability of the complexes. This is supported by NMR and IR spectroscopy, whereby only minor differences are observed between the complexes of the two ligands. If the π-acceptor properties of the pyridine ring were to be altered, then the strength of the CO bond of the carbonyl ligand trans to the pyridine ring should also be altered. This was probed with IR spectroscopy, which showed no significant changes in the C≡O stretching frequency (<2 cm^{-1}, Figures S42−S44) between the complexes of $\mathbf{L^{tri}}$ and $\mathbf{L^{tri}OH}$. This provides further evidence that the observed changes are not due to changes in the electronics of the pyridine ring.

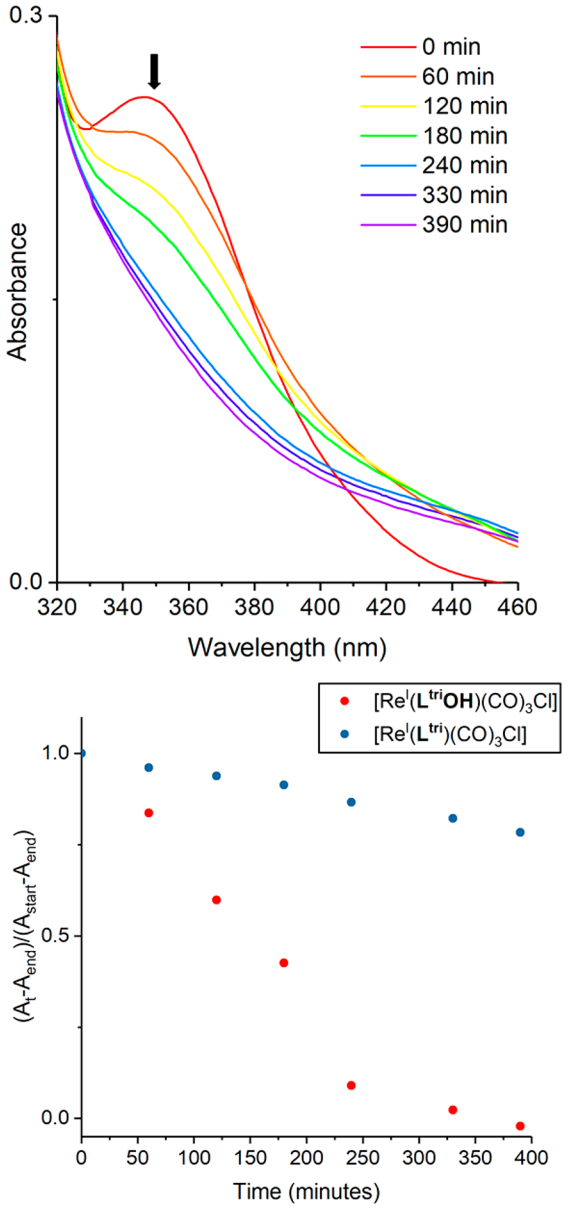

Figure 5. Top: progression of the 360 nm absorption band of a solution of $[Re^I(\mathbf{L^{tri}OH})(CO)_3Cl]$ in DMSO with time under irradiation of 265 nm light. Bottom: Relative change in absorbance at 360 nm for DMSO solutions of $[Re^I(\mathbf{L^{tri}OH})(CO)_3Cl]$ (red) and $[Re^I(\mathbf{L^{tri}})(CO)_3Cl]$ (blue).

The difference in rates can, however, be explained in terms of the steric influence of the CH_2OH group. As described in the structural characterization section, steric effects cause the Re−N(6) bond to be lengthened and weakened in $[Re^I(\mathbf{L^{tri}OH})(CO)_3X]$ relative to $[Re^I(\mathbf{L^{tri}})(CO)_3X]$.

Antimicrobial Activity. The antimicrobial activity of the two pyridyl-triazole ligands and their ruthenium and rhenium complexes was investigated through the determination of minimum inhibitory concentration (MIC) values.[35] All compounds were tested against a range of Gram-positive and Gram-negative bacteria, and the results were compared to the known folate pathway inhibitors sulfamethoxazole (SMX), trimethoprim (TMP), and cotrimoxazole (TMP-SMX, 1:20). A full table of MIC values is given in the Supporting Information (Table S6). All of the bacterial strains tested

DOI: 10.1021/acs.inorgchem.9b01186
Inorg. Chem. XXXX, XXX, XXX−XXX

Table 3. Minimal Inhibitory Concentrations on *S. aureus* of SMX, TMP, BS SMX-TMP, as well as the Rhenium(I) Complexes and Formulations[b] that Showed Activity in This Work[a]

	S. aureus DSM 20231	*S. aureus* ATCC 43300	*S. aureus* BAA 976	*S. aureus* BAA 977
SMX	n.a.[c]	n.a.[c]	n.a.[c]	n.a.[c]
TMP	6.9 [2]	14 [4]	14 [4]	6.9 [2]
Re($\mathbf{L}^{tri}$)Cl	400 [256]	400 [256]	400 [256]	400 [256]
Re($\mathbf{L}^{tri}$)Br	380 [256]	750 [512]	n.a.[c]	190 [128]
Re($\mathbf{L}^{tri}\mathbf{OH}$)Cl	380 [256]	380 [256]	380 [256]	380 [256]
SMX-TMP (20:1)	120:6.0 [32]	960:48 [256]	40:1.5 [8]	40:1.5 [8]
Re($\mathbf{L}^{tri}$)Cl-TMP (20:1)	49:2.5 [32]	98:4.9 [64]	98:4.9 [64]	98:4.9 [64]
Re($\mathbf{L}^{tri}$)Br − TMP (20:1)	46:2.3 [32]	46:2.3 [32]	23:1.2 [16]	46:2.3 [32]

[a]Values are given in μmol L^{-1} and [μg/mL]. [b]Mixtures of the rhenium(I) complexes with TMP in a 20:1 molar ratio. [c]n.a.: not active up to 512 μg/mL.

showed very high resistance against sulfamethoxazole alone, whereas trimethoprim showed high activity against all strains except *Acinetobacter baumannii* and *Pseudomonas aeruginosa*. In most cases, the activity of TMP−SMX was higher on a molar basis than TMP alone. This suggests some cooperative activity despite high levels of resistance to SMX. Three of the synthesized compounds [$Re^{I}(\mathbf{L}^{tri})(CO)_3Cl$], [$Re^{I}(\mathbf{L}^{tri})(CO)_3Br$], and [$Re^{I}(\mathbf{L}^{tri}\mathbf{OH})(CO)_3Cl$] showed modest activity against *S. aureus* (Table 3) and therefore outperformed the parent sulfonamide SMX. Two of the rhenium(I) complexes that showed some activity were then tested in combination with TMP in a 20:1 ratio. This combination was chosen as it is analogous to the plasma concentration of SMX−TMP achieved with the standard clinical formulation.[22]

Interestingly, the activity of the Re-TMP formulations was roughly equal for all strains of *S. aureus* that were tested, including the methicillin-resistant strain, ATCC 4300. In comparison, the standard SMX−TMP formulation gave mixed results, showing good activity against two strains BAA 976 and BAA 977, moderate activity against one strain DSM 20231, and poor activity against MRSA ATCC 4300. These results indicate that such metalated drug fragments may help to increase antimicrobial activity in the cases of high resistance. It is important to note however that the best *per gram* activity against all strains was achieved with TMP alone. These data are therefore not inconsistent with reports that have questioned the increased efficacy of TMP−SMX compared to TMP alone.[36]

CONCLUSION

In summary, a CuAAC click approach has been employed for the functionalization of a known antibiotic drug fragment with metal-containing fragments. The resulting rhenium(I) complexes showed improved performance against MRSA relative to the purely organic drug sulfamethoxazole alone.

Interestingly, the introduction of a CH_2OH group in ortho position to the metal center results in a significantly more labile metal−ligand bond. Subsequent structural characterization of four of the metal complexes indicated this lability is probably due to steric effects, whereby a significant distortion of the octahedral geometry is caused by the introduction of the hydroxymethyl group, as well as a lengthening and weakening of the metal-pyridine bond. Irradiation with 265 nm light increased the rate of ligand exchange for all of the complexes. Under these conditions however, the difference in reaction rates between the two ligands is reduced to 3−8 fold, indicating the weakening of the ligand metal bonds due to steric factors is more important for the "dark" mechanism. These properties could be exploited in the design of future photoactivatible drugs. Antimicrobial testing of our new SMX-derived metal complexes showed encouraging activity against MRSA strains for one Re derivative. However, as treatment options against multiresistant bacteria are generally scarce, this finding certainly merits further attention.

EXPERIMENTAL SECTION

All solvents and reagents were used as received, except for $[Ru(CO)_2Cl_2]_n$[37] and 2-azido-pyridine,[18d] which were prepared according to literature procedures. X-ray crystal structure determination details are provided in Tables S1−S2. The structures were refined with SHELXL[38] within the OLEX-2 graphical user interface.[39] For full instrumentation details, please see the Supporting Information.

***N*-Propargyl-sulfanilamide.** A mixture of sulphanilamide (4.0 g, 23.2 mmol) and K_2CO_3 (3.2 g, 23.2 mmol) in MeCN (120 mL) was heated to 82 °C in a two-necked flask fitted with a dropping funnel. Once this temperature was reached, a solution of propargyl bromide (1.25 mL, 80 wt % solution in toluene, 11.6 mmol) in MeCN (40 mL) was added dropwise over 1 h. Refluxing was then continued for a further 2.5 h before the mixture was allowed to cool to ambient temperature. Water (150 mL) was added, and the mixture was extracted with $CHCl_3$ (3 × 100 mL). The combined organic extracts were dried (Na_2SO_4), filtered, and taken to dryness at reduced pressure to give a waxy yellow solid. This solid was then suspended in DCM/MeCN (16:1, 20 mL), filtered, washed with DCM/MeCN (16:1, 3 × 1 mL), and air-dried. The obtained white solid is analytically pure starting material and can be reused. The filtrate, which contains both the mono- and disubstituted products as well as traces of starting material, was then purified by column chromatography on silica gel (150 mL), eluting with a DCM/MeCN gradient (16:1 → 4:1). Three fractions were then collected. The disubstituted product elutes first (rf = 0.83, 4:1 DCM/MeCN), monosubstituted second (rf = 0.56, 4:1 DCM/MeCN), and finally traces of unreacted starting material (rf = 0.28, 4:1 DCM/MeCN). Yield: 412 mg (1.96 mmol, 17.0% based on propargyl bromide). ESI-MS (pos.) m/z = 232.90 calc. for $[C_9H_{10}N_2O_2S]Na^+$ = 233.03. Elemental analysis calc. for $C_9H_{10}N_2O_2S$ (210.05 g mol^{-1}): C 51.41 H 4.79 N 13.32 S 15.25; found: C 51.44 H 4.74 N 13.48 S 15.17%. ^{1}H NMR (200 MHz, $CDCl_3$): δ (ppm) 7.65 (2H, m, $J_{Hc\text{-}Hb}$ = 8.7 Hz, 2xH_c) 6.69 (2H, m, $J_{Hb\text{-}Hc}$ = 8.7 Hz, 2xH_b) 4.40 (1H, t, $J_{Hd\text{-}He}$ = 6.1 Hz, H_d) 4.13 (2H, s, 2xH_a) 3.80 (2H, dd, $J_{He\text{-}Hd}$ = 6.1 Hz, $J_{He\text{-}Hf}$ = 2.5 Hz, 2xH_e) 2.13 (1H, t, $J_{Hf\text{-}He}$ = 2.5 Hz, H_f). ^{13}C NMR (100 MHz, DMSO-d_6): δ (ppm) 152.6, 128.6, 125.1, 112.6, 79.8, 74.3, 31.9.

2-(4-Methyl-sulfanilamidyl-1*H*-1,2,3-triazol-1-yl)pyridine ($\mathbf{L}^{tri}$). A solution of *N*-propargyl-sulfanilamide (272 mg, 1.30 mmol), 2-azido-pyridine (155 mg, 1.30 mmol), NaOAc (107 mg, 1.30 mmol), and DIPEA (221 μL, 1.30 mmol) in toluene/DMF (9:1 80 mL) was degassed by bubbling with N_2(g) for 20 min. To this solution was

DOI: 10.1021/acs.inorgchem.9b01186
Inorg. Chem. XXXX, XXX, XXX−XXX

then added CuI (247.7 mg, 1.30 mmol) and Cu(s) (8 mg, 0.130 mmol). The resulting suspension was then degassed for a further 20 min before being heated to reflux for 16 h. After this time, a yellow solution had formed with a large amount of brown solid on the walls of the flask. The mixture was allowed to cool to ambient temperature before an aqueous solution of 0.1 M EDTA and 0.1 M NaOH (100 mL) was added. The mixture was stirred at ambient temperature for 1 h and then extracted with a solution of 5% DMF in EtOAc (3 × 150 mL). The organic extracts were dried over Na_2SO_4, filtered, and taken to dryness at reduced pressure to give a beige solid. The solid was then suspended in $CHCl_3$ (80 mL), sonicated, filtered, and washed with $CHCl_3$ (3 × 5 mL). The resulting pale beige solid was air-dried and then further dried in vacuo to give the analytically pure product. Yield: 200 mg, 0.61 mmol, 47%. HR-ESI-MS (pos.) m/z = 331.0968 calc. for $[C_{14}H_{14}N_6O_2S]H^+$ = 331.0977. Elemental analysis calc. for $C_{14}H_{14}N_6O_2S$ (330.36 g mol^{-1}): C 50.90 H 4.27 N 25.44 S 9.71; found: C 50.81 H 4.24 N 25.65 S 9.94%. ^{1}H NMR (300 MHz, DMSO-d_6): δ (ppm) 8.59 (1H, ddd, H_j), 8.48 (1H, s, H_f), 8.05−8.14 (2H, m, H_g and H_h), 7.71 (1H, t, $J_{Hd\text{-}He}$ = 6.0 Hz, H_d), 7.54 (1H, t, $J_{Hi\text{-}Hj}$ = 7.3 Hz, H_i), 7.44 (2H, m, $J_{Hc\text{-}Hb}$ = 8.7 Hz, 2xH_c), 6.57 (2H, m, $J_{Hb\text{-}Hc}$ = 8.7 Hz, 2xH_b), 5.92 (2H, s, H_a), 4.08 (2H, d, $J_{He\text{-}Hd}$ = 6.0 Hz, 2xH_e). ^{13}C{^{1}H} NMR (100 MHz, CDCl3): δ (ppm) 152.7, 149.0, 148.4, 145.1, 140.2, 128.6, 125.1, 124.3, 120.2, 113.6, 112.7, 38.0.

2-(4-Methyl-sulfanilamidyl-1*H*-1,2,3-triazol-1-yl)-6-hydroxymethyl-pyridine (L^{tri}OH). A solution of *N*-propargyl-sulfanilamide (290 mg, 1.38 mmol), 2-azido-6-hydroxymethyl-pyridine (220 mg, 1.47 mmol), NaOAc (115 mg, 1.40 mmol), and DIPEA (238 μL, 1.40 mmol) in toluene/DMF (9:1 80 mL) was degassed by bubbling with N_2(g) for 20 min. To this solution was then added CuI (267 mg, 1.40 mmol) and Cu(s) (9 mg, 0.140 mmol). The resulting suspension was then degassed for a further 20 min before being heated to reflux for 16 h. After this time, an orange solution had formed with a large amount of brown solid on the walls of the flask. The mixture was allowed to cool to ambient temperature before an aqueous solution of 0.1 M EDTA and 0.1 M NaOH (100 mL) was added. The mixture was stirred at ambient temperature for 1 h and then extracted with a solution of 5% DMF in EtOAc (3 × 150 mL). The organic extracts were dried over Na_2SO_4, filtered, and taken to dryness at reduced pressure to give a mixture of a yellow oil and crystalline solid. This was then purified by column chromatography on silica gel (80 mL), eluting with a gradient of MeCN in DCM (20% → 100%). The resulting white solid was dried in vacuo to give the analytically pure product (r.f. = 0.05, MeCN/DCM 1:3). Yield: 232 mg, 0.64 mmol, 47%. HR-ESI-MS (pos.) m/z = 361.1075 calc. for $[C_{15}H_{16}N_6O_3S]H^+$ = 361.1083. Elemental analysis calc. for $C_{15}H_{16}N_6O_3S$ (360.39 g mol^{-1}): C 49.99 H 4.48 N 23.32, S 8.90; found: C 49.83 H 4.47 N 23.57 S 9.08%. ^{1}H NMR (400 MHz, DMSO-d_6): δ (ppm) 8.45 (1H, s, H_f), 8.09 (1H, t, $J_{Hh\text{-}Hg}$ = $J_{Hh\text{-}Hi}$ = 7.8 Hz H_h), 7.92 (1H, d, $J_{Hg\text{-}Hh}$ = 8.0 Hz, H_g), 7.70 (1H, br. s, H_d), 7.58 (1H, d, $J_{Hi\text{-}Hh}$ = 7.6 Hz, H_i), 7.44 (2H, m, $J_{Hc\text{-}Hb}$ = 8.7 Hz, 2xH_c), 6.59 (2H, m, $J_{Hb\text{-}Hc}$ = 8.7 Hz, 2xH_b), 5.91 (2H, s, H_a), 5.60 (1H, t, $J_{Hl\text{-}Hk}$ = 5.1 Hz, H_l) 4.64 (2H, d, $J_{Hk\text{-}Hl}$ = 5.1 Hz, 2xH_k) 4.07 (2H, br. s, 2xH_e) ^{13}C{^{1}H} NMR (100 MHz, DMSO-d_6): δ (ppm) 162.1, 152.6, 147.4, 145.1, 140.4, 128.5, 125.0, 120.3, 120.1, 112.6, 111.3, 63.7, 38.0. A small sample of **L^{tri}OH** was dissolved in MeCN-d_3 and allowed to slowly evaporate in an NMR tube, resulting in colorless rod-shaped crystals suitable for X-ray crystallography.

[Re^I(L^{tri})(CO)$_3$Cl]. A suspension of $[Re^I(CO)_5Cl]$ (103 mg, 0.28 mmol) and **L^{tri}** (94 mg, 0.28 mmol) in EtOH (25 mL) was degassed by bubbling with N_2(g) before being heated to reflux under a nitrogen atmosphere for 18 h. During this time, the suspension had mostly cleared to give a yellow solution. The mixture was allowed to cool to ambient temperature, and a small amount of solid was filtered off. The filtrate was then taken to dryness at reduced pressure to give a waxy yellow solid. This was then purified by column chromatography on silica gel (70 mL), eluting with EtOH/$CHCl_3$ (1:8). The bright yellow band (rf = 0.18) was collected. The solvents were then removed at reduced pressure giving the analytically pure product as a yellow oil. Yield: 153 mg, 0.24 mmol, 86%. HR-ESI-MS (pos.) m/z = 601.0320 calc. for $[C_{17}H_{14}N_6O_5ReS]^+$ = 601.0303; m/z = 1273.0073 calc. for $[C_{17}H_{14}N_6ClO_5ReS]_2H^+$ = 1273.0037. Elemental analysis calc. for $C_{17}H_{14}N_6ClO_5ReS$ (636.06 g mol^{-1}): C 32.10 H 2.22 N 13.21 S 5.04; found: C 32.23 H 2.38 N 13.23 S 4.99%. ^{1}H NMR (300 MHz, CD_3CN): δ (ppm) 8.90 (1H, ddd, $J_{Hj\text{-}Hi}$ = 5.6 Hz, H_j), 8.51 (1H, s, H_f) 8.31 (1H, ddd, $J_{Hh\text{-}Hg}$ = 8.3 Hz, $J_{Hh\text{-}Hi}$ = 7.7 Hz, H_h), 7.99 (1H, dt, $J_{Hg\text{-}Hh}$ = 8.2 Hz, H_g), 7.63 (1H, td, $J_{Hi\text{-}Hh}$ = 7.7 Hz, H_i), 7.50 (2H, m, $J_{Hc\text{-}Hb}$ = 8.7 Hz, 2xH_c), 6.64 (2H, m, $J_{Hb\text{-}Hc}$ = 8.7 Hz, 2xH_b), 6.11 (1H, t, $J_{Hd\text{-}He}$ = 6.5 Hz, H_d), 4.74 (2H, s, H_a) 4.28 (2H, d, $J_{He\text{-}Hd}$ = 6.5 Hz, 2xH_e) ^{13}C{^{1}H} NMR (100 MHz, CD_3CN): δ (ppm) 196.4, 195.4, 188.0, 152.3, 152.0, 148.3, 146.9, 142.6, 128.8, 126.1, 125.9, 122.9, 114.3, 113.0, 37.6. ATR-IR (cm^{-1}): 2368 (w), 2025 (s, CO), 1904 (s, br., CO), 1625 (w), 1597 (m), 1501 (w), 1456 (w), 1319 (m, br.), 1151 (s), 1096 (m), 1066 (m), 834 (w), 775 (m), 683 (w). Pale yellow needle-shaped single crystals of $[Re^I(\mathbf{L^{tri}})(CO)_3Cl]$·acteone (polymorph A, $P2_1/c$) suitable for single crystal X-ray diffraction were grown by vapor diffusion of hexane into a solution of $[Re^I(\mathbf{L^{tri}})(CO)_3Cl]$ in acetone. Highlighter-yellow, plate-shaped single crystals of $[Re^I(\mathbf{L^{tri}})(CO)_3Cl]$ (polymorph B, *Pn*) suitable for single crystal X-ray diffraction were grown by slow evaporation of a solution of $[Re^I(\mathbf{L^{tri}})(CO)_3Cl]$ in MeOH.

[Re^I(Ltri)(CO)$_3$Br]. A suspension of $[Re^I(CO)_5Br]$ (98 mg, 0.24 mmol) and **L^{tri}** (80 mg, 0.24 mmol) in EtOH (25 mL) was degassed by bubbling with N_2(g) before being heated to reflux under a nitrogen atmosphere for 40 h. During this time, the suspension cleared to give a yellow solution. The mixture was allowed to cool to ambient temperature and then taken to dryness at reduced pressure to give a waxy yellow solid. Elemental analysis calc. for $C_{17}H_{14}BrN_6O_5ReS$ (679.95 g mol^{-1}): C 30.01, H 2.07, N 12.35, S 4.71; found: C 30.38 H 2.35 N 11.99 S 5.08%. HR-ESI-MS (pos.) m/z = 680.9542 calc. for $[C_{17}H_{14}BrN_6O_6ReS]H^+$ = 680.9547; m/z = 601.0320 calc. for $[C_{17}H_{14}N_6O_6ReS]^+$ = 601.0303. ^{1}H NMR (300 MHz, CD_3CO): δ (ppm) 9.06 (1H, dt, $J_{Hj\text{-}Hi}$ = 5.5 Hz, H_j), 9.01 (1H, s, H_f), 8.51 (2H, m, H_h and H_g), 7.82 (1H, m, H_i), 7.56 (2H, m, $J_{Hc\text{-}Hb}$ = 8.9 Hz, 2xH_c), 6.97 (1H, t, $J_{Hd\text{-}He}$ = 6.4 Hz, H_d), 6.73 (2H, m, $J_{Hb\text{-}Hc}$ = 8.9 Hz, 2xH_b), 5.42 (2H, br. s, 2xH_a), 4.36 (2H, d, $J_{He\text{-}Hd}$ = 6.4 Hz, 2xH_e). ^{13}C{^{1}H} NMR (100 MHz, CD_3CO): δ (ppm) 197.4, 196.3, 188.8, 153.7, 153.5, 150.0, 148.5, 143.8, 130.0, 129.3, 127.3, 124.3, 120.7, 115.5, 114.1, 38.9. ATR-IR (cm^{-1}): 2976 (w), 2365 (w), 2025 (s, CO), 1902 (s, br., CO), 1622 (w), 1597 (m), 1495 (w), 1456 (w), 1315 (m, br.), 1151 (s), 1067 (m), 837 (w), 771 (m), 681 (w). Highlighter-yellow, needle-shaped single crystals of $[Re^I(\mathbf{L^{tri}})(CO)_3Br]$ suitable for single crystal X-ray diffraction were grown by slow evaporation of a solution of $[Re^I(\mathbf{L^{tri}})(CO)_3Br]$ in MeOH.

[Ru^{II}(L^{tri})(CO)$_2$Cl$_2$]. A suspension of $[Ru^{II}(CO)_2Cl_2]_n$ (69 mg, 0.30 mmol) and **L^{tri}** (100 mg, 0.30 mmol) in EtOH (30 mL) was degassed by bubbling with N_2(g) before being heated to reflux under a nitrogen atmosphere for 18 h. During this time, the suspension cleared to give a yellow solution. The mixture was allowed to cool to ambient temperature and then taken to dryness at reduced pressure to give a waxy yellow solid. This was then purified by reverse-phase (C18) column chromatography using a CombiFlash Rf system with a THF/H_2O gradient (5% → 95%). The product eluted with 25% THF. The solution was then concentrated to approximately half the volume by rotary evaporation, which caused a yellow precipitate to form. The solution was stored at 4 °C for 1 h to allow further precipitation then filtered and washed with a small amount of water. The product was first air-dried then further dried in vacuo. Yield: 106 mg, 0.17 mmol, 67%. HR-ESI-MS (pos.) m/z = 522.9542 calc. for $[C_{16}H_{14}N_6ClO_4RuS]^+$ = 522.9542 ^{1}H NMR (300 MHz, CD_3CN): δ (ppm) 9.07 (1H, dd, $J_{Hj\text{-}Hi}$ = 6.3 Hz, H_j), 8.58 (1H, s, H_f), 8.38 (1H, td, $J_{Hh\text{-}Hi}$ = $J_{Hh\text{-}Hg}$ = 8.3 Hz, $J_{Hh\text{-}Hj}$ = 1.6 Hz, H_h), 8.04 (1H, d, $J_{Hg\text{-}Hh}$ = 8.3 Hz, H_g), 7.79 (1H, t, $J_{Hi\text{-}Hh}$ = $J_{Hi\text{-}Hj}$ = 8.3 Hz, H_i), 7.50 (2H, m, $J_{Hc\text{-}Hb}$ = 8.7 Hz, 2xH_c), 6.66 (2H, m, $J_{Hb\text{-}Hc}$ = 8.7 Hz, 2xH_b), 6.11 (1H, t, $J_{Hd\text{-}He}$ = 6.4 Hz, H_d), 4.75 (2H, s, 2xH_a) 4.33 (2H, d, $J_{He\text{-}Hd}$ = 6.4 Hz, 2xH_e). ^{13}C{^{1}H} NMR (100 MHz, CD_3CN): δ (ppm) 196.62, 196.32, 153.56, 153.34, 150.18, 147.09, 144.49, 130.07, 127.89, 127.30, 124.69, 116.04, 114.49, 39.03. ATR-IR (cm^{-1}): 3129 (w), 2360 (w), 2069 (s, CO), 2019 (s, CO), 1613 (m), 1596 (s), 1498 (s), 1449 (m), 1312 (m), 1161 (s), 1073 (s), 836 (m), 783 (s), 687 (m), 675 (m), 629 (m). Colorless, needle-shaped single crystals of suitable

DOI: 10.1021/acs.inorgchem.9b01186
Inorg. Chem. XXXX, XXX, XXX−XXX

for single crystal X-ray diffraction were grown by vapor diffusion of Et_2O into a solution of $[Ru^{II}(L^{tri})(CO)_2Cl_2]$ in acetone.

$[Re^{I}(L^{tri}OH)(CO)_3Cl]$. A suspension of $[Re^{I}(CO)_5Cl]$ (80.3 mg, 0.22 mmol) and **$L^{tri}OH$** (80 mg, 0.22 mmol) in EtOH (25 mL) was degassed by bubbling with N_2(g) before being heated to reflux under a nitrogen atmosphere for 18 h. During this time, the suspension cleared to give a yellow solution. The mixture was allowed to cool to ambient temperature, and the solution was taken to dryness at reduced pressure to give a yellow oil. This was then purified by column chromatography on silica gel (40 mL), eluting with EtOAc/hexane (gradient 1:1 → 1:0). The bright yellow band (rf = 0.4, EtOAc) was collected. The solvents were then removed at reduced pressure giving the analytically pure product as a yellow solid. Yield: 127 mg, 0.19 mmol, 86%. HR-ESI-MS (pos.) m/z = 631.0410 calc. for $[C_{18}H_{16}N_6O_6ReS]^+$ = 631.0403; m/z = 672.0668 calc. for $[C_{18}H_{16}N_6O_6ReS]{\cdot}MeCN^+$ = 672.0668; m/z = 1333.0209 calc. for $\{[C_{18}H_{16}N_6O_6ReS]_2H\}^+$ = 1333.0242. Elemental analysis calc. for $[C_{18}H_{16}ClN_6O_6ReS]{\cdot}0.5EtOAc$ (710.14 g mol^{-1}): C 33.83 H 2.84 N 11.83 S 4.51; found: C 33.93 H 2.92 N 11.83 S 4.43%. ^1H NMR (400 MHz, CD_3CO): δ (ppm) 8.98 (1H, s, H_f), 8.48 (1H, t, $J_{Hh\text{-}Hi} = J_{Hh\text{-}Hg}$ = 8.0 Hz, H_h), 8.34 (1H, d, $J_{Hg\text{-}Hh}$ = 7.9 Hz, H_g), 8.11 (1H, d, $J_{Hi\text{-}Hh}$ = 7.9 Hz, H_i), 7.56 (2H, m, $J_{Hc\text{-}Hb}$ = 8.7 Hz, 2xH_c), 6.97 (1H, t, $J_{Hd\text{-}He}$ = 6.4 Hz, H_d), 6.72 (2H, m, $J_{Hb\text{-}Hc}$ = 8.7 Hz, 2xH_b), 5.40 (1H, t, $J_{Hl\text{-}Hk}$ = 5.4 Hz, H_l), 5.07 (2H, t, $J_{Hk\text{-}Hl}$ = 5.5 Hz, 2xH_k), 4.37 (2H, d, $J_{He\text{-}Hd}$ = 6.4 Hz, 2xH_e). $^{13}C\{^1H\}$ NMR (100 MHz, CD_3CO): δ (ppm) 198.1, 195.8, 188.6, 165.1, 153.5, 150.1, 148.7, 143.7, 130.0, 127.4, 127.3, 124.3, 123.3, 114.0, 113.5, 68.7, 39.0. ATR-IR (cm^{-1}): 2367 (m), 2027 (s, CO), 1902 (s, br., CO), 1626 (w), 1597 (m), 1479 (w), 1320 (m, br.), 1146 (s), 1080 (m), 837 (w), 800 (w), 681 (m).

$[Re^{I}(L^{tri}OH)(CO)_3Br]$. A suspension of $[Re^{I}(CO)_5Br]$ (90.2 mg, 0.22 mmol) and **$L^{tri}OH$** (80 mg, 0.22 mmol) in EtOH (25 mL) was degassed by bubbling with N_2(g) before being heated to reflux under a nitrogen atmosphere for 18 h. During this time, the suspension cleared to give a yellow solution. The mixture was allowed to cool to ambient temperature, and the solution was taken to dryness at reduced pressure to give a yellow oil. Further drying under high vacuum caused this oil to solidify, giving the analytically pure product as a yellow powder. Yield: 156.3 mg, 0.22 mmol, 100%. HR-ESI-MS (pos.) m/z = 631.0420 calc. for $[C_{18}H_{16}BrN_6O_6ReS]^+$ = 631.0403; m/z = 672.0682 calc. for $[C_{18}H_{16}BrN_6O_6ReS]{\cdot}MeCN^+$ = 672.0668; m/z = 710.9664 calc. for $[C_{18}H_{16}BrN_6O_6ReS]H^+$ = 710.9648. Elemental analysis calc. for $[C_{18}H_{16}BrN_6O_6ReS]{\cdot}H_2O$ (728.55 g mol^{-1}): C 29.68, H 2.49, N 11.54, S 4.40; found: C 29.56, H 2.44, N 11.48, S 4.39%. ^1H NMR (400 MHz, CD_3CO): δ (ppm) 8.98 (1H, s, H_f), 8.47 (1H, t $J_{Hh\text{-}Hi} = J_{Hh\text{-}Hg}$ = 8.0 Hz, H_h), 8.35 (1H, d, $J_{Hg\text{-}Hh}$ = 8.1 Hz, H_g), 8.11 (1H, d, $J_{Hi\text{-}Hh}$ = 7.9 Hz, H_i), 7.56 (2H, m, $J_{Hc\text{-}Hb}$ = 8.7 Hz, 2xH_c), 6.97 (1H, t, $J_{Hd\text{-}He}$ = 6.5 Hz, H_d), 6.72 (2H, m, $J_{Hb\text{-}Hc}$ = 8.7 Hz, H_b), 5.40 (1H, t, $J_{Hl\text{-}Hk}$ = 5.4 Hz, H_l) 5.05 (2H, qd, $J_{Hk\text{-}Hl}$ = 6.1 Hz, 2xH_k), 4.37 (2H, d, $J_{He\text{-}Hd}$ = 6.4 Hz, 2xH_e) $^{13}C\{^1H\}$ NMR (100 MHz, CD_3CO): δ (ppm) 197.5, 195.5, 187.8, 165.3, 153.5, 150.2, 148.7, 143.6, 130.0, 127.4, 124.3, 123.3, 114.1, 113.4, 68.8, 39.0. ATR-IR (cm^{-1}): 2365 (m), 2028 (s, CO), 1904 (s, br., CO), 1624 (w), 1597 (m), 1477 (w), 1315 (m, br.), 1150 (s), 1070 (m) 835 (w), 879 (w), 679 (w). Yellow rod-shaped single crystals of suitable for single crystal X-ray diffraction were grown by vapor diffusion of hexane into a solution of $[Re^{I}(L^{tri}OH)(CO)_3Br]$ in EtOH/acetone (1:1).

$[Ru^{II}(L^{tri}OH)(CO)_2Cl_2]$. A suspension of $[Ru^{II}(CO)_2Cl_2]_n$ (69 mg, 0.30 mmol) and **$L^{tri}OH$** (100 mg, 0.30 mmol) in EtOH (30 mL) was degassed by bubbling with N_2(g) before being heated to reflux under a nitrogen atmosphere for 18 h. During this time, the suspension cleared to give a yellow solution. The mixture was allowed to cool to ambient temperature and then taken to dryness at reduced pressure to give a waxy yellow solid. This yellow solid was then purified by column chromatography on silica gel (50 mL), eluting with acetone/hexane (2:1) to give a waxy bright yellow solid (rf = 0.2, acetone/hexane 2:1). Yield: 88 mg (0.150 mmol 50%). HR-ESI-MS (pos.) m/z = 516.9869 calc. for $[C_{17}H_{15}N_6O_5ReS]^+$ = 516.9867; m/z = 552.9634 calc. for $[C_{17}H_{16}ClN_6O_5ReS]^+$ = 552.9630; m/z = 1178.8713 calc. for $\{[C_{17}H_{16}ClN_6O_5ReS]_2H\}^+$ = 1178.8709. ^1H NMR (300 MHz, acetone-d_6): δ (ppm) 9.07 (1H, s, H_f), 8.55 (1H, t, $J_{Hh\text{-}Hi} = J_{Hh\text{-}Hg}$ = 8.0 Hz, H_h), 8.40 (1H, d, $J_{Hg\text{-}Hh}$ = 8.5 Hz, H_g), 8.17 (1H, d, $J_{Hi\text{-}Hh}$ = 7.9 Hz, H_i), 7.57 (2H, m, $J_{Hc\text{-}Hb}$ = 8.8 Hz, 2xH_c), 7.01 (1H, t, $J_{Hd\text{-}He}$ = 6.4 Hz, H_d), 6.73 (2H, m, $J_{Hb\text{-}Hc}$ = 8.8 Hz, 2xH_b), 5.51 (1H, t, $J_{Hl\text{-}Hk}$ = 5.6 Hz, H_l) 5.42 (2H, br. s, H_a), 5.30 (2H, d, $J_{Hk\text{-}Hl}$ = 5.4 Hz, 2xH_k), 4.42 (2H, d, $J_{He\text{-}Hd}$ = 6.4 Hz, 2xH_e). $^{13}C\{^1H\}$ NMR (100 MHz, acetone-d_6): δ (ppm) 196.9, 196.6, 164.6, 153.5, 150.8, 147.3, 144.3, 130.0, 127.4, 124.7, 123.9, 114.2, 113.8, 67.0, 39.2. ATR-IR (cm^{-1}): 2926 (w), 2365 (m), 2075 (s, CO), 2016 (s, CO), 1622 (w), 1595 (m), 1475 (w), 1317 (m, br.), 1151 (s), 1082 (s), 839 (m), 800 (m), 679 (m), 631 (w).

■ ASSOCIATED CONTENT

Supporting Information

The Supporting Information is available free of charge on the ACS Publications website at DOI: 10.1021/acs.inorgchem.9b01186.

Instrument details, crystallographic data, additional structural diagrams, IR spectra, UV−vis spectra, MIC data, and biological procedures, as well as NMR spectra and NMR numbering schemes (PDF)

Accession Codes

CCDC 1909703−1909708 contain the supplementary crystallographic data for this paper. These data can be obtained free of charge via www.ccdc.cam.ac.uk/data_request/cif, or by emailing data_request@ccdc.cam.ac.uk, or by contacting The Cambridge Crystallographic Data Centre, 12 Union Road, Cambridge CB2 1EZ, UK; fax: +44 1223 336033.

■ AUTHOR INFORMATION

Corresponding Author

*E-mail: nils.metzler-nolte@rub.de.

ORCID

Reece G. Miller: 0000-0002-2687-5572
Melissa Vázquez-Hernández: 0000-0003-2527-9135
Julia E. Bandow: 0000-0003-4100-8829
Nils Metzler-Nolte: 0000-0001-8111-9959

Notes

The authors declare no competing financial interest.

■ ACKNOWLEDGMENTS

We are grateful to the Alexander von Humboldt foundation for the award of a research fellowship to R.G.M.

■ REFERENCES

(1) (a) Taubes, G. The Bacteria Fight Back. *Science* **2008**, *321* (5887), 356−361. (b) Levy, S. B.; Marshall, B. Antibacterial resistance worldwide: causes, challenges and responses. *Nat. Med.* **2004**, *10*, S122. (c) Blair, J. M. A.; Webber, M. A.; Baylay, A. J.; Ogbolu, D. O.; Piddock, L. J. V. Molecular mechanisms of antibiotic resistance. *Nat. Rev. Microbiol.* **2015**, *13*, 42.

(2) (a) Peacock, S. J.; Paterson, G. K. Mechanisms of Methicillin Resistance in Staphylococcus aureus. *Annu. Rev. Biochem.* **2015**, *84* (1), 577−601. (b) David, M. Z.; Daum, R. S. Community-Associated Methicillin-Resistant *Staphylococcus aureus*: Epidemiology and Clinical Consequences of an Emerging Epidemic. *Clin. Microbiol. Rev.* **2010**, *23* (3), 616−687.

(3) Brötz-Oesterhelt, H.; Brunner, N. A. How many modes of action should an antibiotic have? *Curr. Opin. Pharmacol.* **2008**, *8* (5), 564−573.

(4) (a) Patra, M.; Wenzel, M.; Prochnow, P.; Pierroz, V.; Gasser, G.; Bandow, J. E.; Metzler-Nolte, N. An organometallic structure-activity relationship study reveals the essential role of a $Re(CO)_3$ moiety in the activity against gram-positive pathogens including MRSA. *Chem. Sci.* **2015**, *6* (1), 214−224. (b) Hartinger, C. G.; Metzler-Nolte, N.;

DOI: 10.1021/acs.inorgchem.9b01186
Inorg. Chem. XXXX, XXX, XXX−XXX

Dyson, P. J. Challenges and Opportunities in the Development of Organometallic Anticancer Drugs. *Organometallics* **2012**, *31* (16), 5677−5685. (c) Bandow, J. E.; Metzler-Nolte, N. New Ways of Killing the Beast: Prospects for Inorganic−Organic Hybrid Nanomaterials as Antibacterial Agents. *ChemBioChem* **2009**, *10* (18), 2847−2850. (d) Mjos, K. D.; Orvig, C. Metallodrugs in Medicinal Inorganic Chemistry. *Chem. Rev.* **2014**, *114* (8), 4540−4563. (e) Guo, Z.; Sadler, P. J. Metals in Medicine. *Angew. Chem., Int. Ed.* **1999**, *38* (11), 1512−1531. (f) Gasser, G.; Metzler-Nolte, N. The potential of organometallic complexes in medicinal chemistry. *Curr. Opin. Chem. Biol.* **2012**, *16* (1), 84−91. (g) Wenzel, M.; Patra, M.; Senges, C. H. R.; Ott, I.; Stepanek, J. J.; Pinto, A.; Prochnow, P.; Vuong, C.; Langklotz, S.; Metzler-Nolte, N.; Bandow, J. E. Analysis of the Mechanism of Action of Potent Antibacterial Hetero-tri-organometallic Compounds: A Structurally New Class of Antibiotics. *ACS Chem. Biol.* **2013**, *8* (7), 1442−1450. (h) Patra, M.; Gasser, G.; Bobukhov, D.; Merz, K.; Shtemenko, A. V.; Metzler-Nolte, N. Sequential insertion of three different organometallics into a versatile building block containing a PNA backbone. *Dalton Trans.* **2010**, *39* (24), 5617−5619.

(5) Patra, M.; Gasser, G.; Metzler-Nolte, N. Small organometallic compounds as antibacterial agents. *Dalton Trans.* **2012**, *41* (21), 6350−6358.

(6) (a) Knoll, J. D.; Turro, C. Control and utilization of ruthenium and rhodium metal complex excited states for photoactivated cancer therapy. *Coord. Chem. Rev.* **2015**, *282*−*283*, 110−126. (b) McKenzie, L. K.; Bryant, H. E.; Weinstein, J. A. Transition metal complexes as photosensitisers in one- and two-photon photodynamic therapy. *Coord. Chem. Rev.* **2019**, *379*, 2. (c) Higgins, S. L. H.; Tucker, A. J.; Winkel, B. S. J.; Brewer, K. J. Metal to ligand charge transfer induced DNA photobinding in a Ru(II)−Pt(II) supramolecule using red light in the therapeutic window: a new mechanism for DNA modification. *Chem. Commun.* **2012**, *48* (1), 67−69.

(7) (a) Bruijnincx, P. C. A.; Sadler, P. J. New trends for metal complexes with anticancer activity. *Curr. Opin. Chem. Biol.* **2008**, *12* (2), 197−206. (b) Graf, N.; Lippard, S. J. Redox activation of metal-based prodrugs as a strategy for drug delivery. *Adv. Drug Delivery Rev.* **2012**, *64* (11), 993−1004.

(8) Renfrew, A. K. Transition metal complexes with bioactive ligands: mechanisms for selective ligand release and applications for drug delivery. *Metallomics* **2014**, *6* (8), 1324−1335.

(9) (a) Raszeja, L.; Maghnouj, A.; Hahn, S.; Metzler-Nolte, N. A Novel Organometallic ReI Complex with Favourable Properties for Bioimaging and Applicability in Solid-Phase Peptide Synthesis. *ChemBioChem* **2011**, *12* (3), 371−376. (b) Raszeja, L. J.; Siegmund, D.; Cordes, A. L.; Güldenhaupt, J.; Gerwert, K.; Hahn, S.; Metzler-Nolte, N. Asymmetric rhenium tricarbonyl complexes show superior luminescence properties in live cell imaging. *Chem. Commun.* **2017**, *53* (5), 905−908.

(10) (a) Yang, J.; Zhao, J.-X.; Cao, Q.; Hao, L.; Zhou, D.; Gan, Z.; Ji, L.-N.; Mao, Z.-W. Simultaneously Inducing and Tracking Cancer Cell Metabolism Repression by Mitochondria-Immobilized Rhenium(I) Complex. *ACS Appl. Mater. Interfaces* **2017**, *9* (16), 13900−13912. (b) König, M.; Siegmund, D.; Raszeja, L. J.; Prokop, A.; Metzler-Nolte, N. Resistance-breaking profiling and gene expression analysis on an organometallic ReI−phenanthridine complex reveal parallel activation of two apoptotic pathways. *MedChemComm* **2018**, *9* (1), 173−180.

(11) Rostovtsev, V. V.; Green, L. G.; Fokin, V. V.; Sharpless, K. B. A Stepwise Huisgen Cycloaddition Process: Copper(I)-Catalyzed Regioselective "Ligation" of Azides and Terminal Alkynes. *Angew. Chem., Int. Ed.* **2002**, *41* (14), 2596−2599.

(12) Tornøe, C. W.; Christensen, C.; Meldal, M. Peptidotriazoles on Solid Phase: [1,2,3]-Triazoles by Regiospecific Copper(I)-Catalyzed 1,3-Dipolar Cycloadditions of Terminal Alkynes to Azides. *J. Org. Chem.* **2002**, *67* (9), 3057−3064.

(13) Liang, L.; Astruc, D. The copper(I)-catalyzed alkyne-azide cycloaddition (CuAAC) "click" reaction and its applications. An overview. *Coord. Chem. Rev.* **2011**, *255* (23), 2933−2945.

(14) (a) Hoffknecht, B. C.; Prochnow, P.; Bandow, J. E.; Metzler-Nolte, N. Influence of metallocene substitution on the antibacterial activity of multivalent peptide conjugates. *J. Inorg. Biochem.* **2016**, *160*, 246−249. (b) Hong, V.; Presolski, S. I.; Ma, C.; Finn, M. G. Analysis and Optimization of Copper-Catalyzed Azide−Alkyne Cycloaddition for Bioconjugation. *Angew. Chem., Int. Ed.* **2009**, *48* (52), 9879−9883. (c) McKay, C. S.; Finn, M. G. Click Chemistry in Complex Mixtures: Bioorthogonal Bioconjugation. *Chem. Biol.* **2014**, *21* (9), 1075−1101. (d) Lutz, J.-F.; Zarafshani, Z. Efficient construction of therapeutics, bioconjugates, biomaterials and bioactive surfaces using azide−alkyne "click" chemistry. *Adv. Drug Delivery Rev.* **2008**, *60* (9), 958−970.

(15) Astruc, D.; Liang, L.; Rapakousiou, A.; Ruiz, J. Click Dendrimers and Triazole-Related Aspects: Catalysts, Mechanism, Synthesis, and Functions. A Bridge between Dendritic Architectures and Nanomaterials. *Acc. Chem. Res.* **2012**, *45* (4), 630−640.

(16) (a) Li, N.; Binder, W. H. Click-chemistry for nanoparticle-modification. *J. Mater. Chem.* **2011**, *21* (42), 16717−16734. (b) Poonthiyil, V.; Lindhorst, T. K.; Golovko, V. B.; Fairbanks, A. J. Recent applications of click chemistry for the functionalization of gold nanoparticles and their conversion to glyco-gold nanoparticles. *Beilstein J. Org. Chem.* **2018**, *14*, 11−24.

(17) (a) Kumar, S. V.; Lo, W. K. C.; Brooks, H. J. L.; Hanton, L. R.; Crowley, J. D. Antimicrobial Properties of Mono- and Di-*fac*-rhenium Tricarbonyl 2-Pyridyl-1,2,3-triazole Complexes. *Aust. J. Chem.* **2016**, *69* (5), 489−498. (b) Kumar, S. V.; Scottwell, S. Ø.; Waugh, E.; McAdam, C. J.; Hanton, L. R.; Brooks, H. J. L.; Crowley, J. D. Antimicrobial Properties of Tris(homoleptic) Ruthenium(II) 2-Pyridyl-1,2,3-triazole "Click" Complexes against Pathogenic Bacteria, Including Methicillin-Resistant Staphylococcus aureus (MRSA). *Inorg. Chem.* **2016**, *55* (19), 9767−9777.

(18) (a) Bertrand, H. C.; Clède, S.; Guillot, R.; Lambert, F.; Policar, C. Luminescence Modulations of Rhenium Tricarbonyl Complexes Induced by Structural Variations. *Inorg. Chem.* **2014**, *53* (12), 6204−6223. (b) Mydlak, M.; Bizzarri, C.; Hartmann, D.; Sarfert, W.; Schmid, G.; De Cola, L. Positively Charged Iridium(III) Triazole Derivatives as Blue Emitters for Light-Emitting Electrochemical Cells. *Adv. Funct. Mater.* **2010**, *20* (11), 1812−1820. (c) Happ, B.; Friebe, C.; Winter, A.; Hager, M. D.; Hoogenboom, R.; Schubert, U. S. 2-(1 H-1,2,3-Triazol-4-yl)-Pyridine Ligands as Alternatives to 2,2′-Bipyridines in Ruthenium(II) Complexes. *Chem. - Asian J.* **2009**, *4* (1), 154−163. (d) Lo, W. K. C.; Huff, G. S.; Cubanski, J. R.; Kennedy, A. D. W.; McAdam, C. J.; McMorran, D. A.; Gordon, K. C.; Crowley, J. D. Comparison of Inverse and Regular 2-Pyridyl-1,2,3-triazole "Click" Complexes: Structures, Stability, Electrochemical, and Photophysical Properties. *Inorg. Chem.* **2015**, *54* (4), 1572−1587.

(19) (a) Ching, H. Y. V.; Wang, X.; He, M.; Perujo Holland, N.; Guillot, R.; Slim, C.; Griveau, S.; Bertrand, H. C.; Policar, C.; Bedioui, F.; Fontecave, M. Rhenium Complexes Based on 2-Pyridyl-1,2,3-triazole Ligands: A New Class of CO_2 Reduction Catalysts. *Inorg. Chem.* **2017**, *56* (5), 2966−2976. (b) Hohloch, S.; Suntrup, L.; Sarkar, B. Arene−Ruthenium(II) and − Iridium(III) Complexes with "Click"-Based Pyridyl-triazoles, Bis-triazoles, and Chelating Abnormal Carbenes: Applications in Catalytic Transfer Hydrogenation of Nitrobenzene. *Organometallics* **2013**, *32* (24), 7376−7385.

(20) Valencia, M.; Müller-Bunz, H.; Gossage, R. A.; Albrecht, M. Enhanced product selectivity promoted by remote metal coordination in acceptor-free alcohol dehydrogenation catalysis. *Chem. Commun.* **2016**, *52* (16), 3344−3347.

(21) Yun, M.-K.; Wu, Y.; Li, Z.; Zhao, Y.; Waddell, M. B.; Ferreira, A. M.; Lee, R. E.; Bashford, D.; White, S. W. Catalysis and Sulfa Drug Resistance in Dihydropteroate Synthase. *Science* **2012**, *335* (6072), 1110.

(22) Foltzer, M. A.; Reese, R. E. Trimethoprim-Sulfamethoxazole and Other Sulfonamides. *Med. Clin. North Am.* **1987**, *71* (6), 1177−1194.

(23) Kompis, I. M.; Islam, K.; Then, R. L. DNA and RNA Synthesis: Antifolates. *Chem. Rev.* **2005**, *105* (2), 593−620.

(24) Raz, R.; Chazan, B.; Kennes, Y.; Colodner, R.; Rottensterich, E.; Dan, M.; Lavi, I.; Stamm, W. Empiric Use of Trimethoprim-

DOI: 10.1021/acs.inorgchem.9b01186
Inorg. Chem. XXXX, XXX, XXX−XXX

Sulfamethoxazole (TMP-SMX) in the Treatment of Women with Uncomplicated Urinary Tract Infections, in a Geographical Area with a High Prevalence of TMP-SMX−Resistant Uropathogens. *Clin. Infect. Dis.* **2002**, *34* (9), 1165−1169.
(25) Ericsson, C. D.; DuPont, H. L.; Mathewson, J. J.; West, M.; Johnson, P. C.; Bitsura, J. M. Treatment of traveler's diarrhea with sulfamethoxazole and trimethoprim and loperamide. *JAMA* **1990**, *263* (2), 257−261.
(26) Paul, M.; Bishara, J.; Yahav, D.; Goldberg, E.; Neuberger, A.; Ghanem-Zoubi, N.; Dickstein, Y.; Nseir, W.; Dan, M.; Leibovici, L. Trimethoprim-sulfamethoxazole versus vancomycin for severe infections caused by meticillin resistant Staphylococcus aureus: randomised controlled trial. *BMJ.* **2015**, *350*, No. h2219.
(27) (a) Sköld, O. Sulfonamide resistance: mechanisms and trends. *Drug Resist. Updates* **2000**, *3* (3), 155−160. (b) LaPlante, K. L.; Leonard, S. N.; Andes, D. R.; Craig, W. A.; Rybak, M. J. Activities of Clindamycin, Daptomycin, Doxycycline, Linezolid, Trimethoprim-Sulfamethoxazole, and Vancomycin against Community-Associated Methicillin-Resistant *Staphylococcus aureus* with Inducible Clindamycin Resistance in Murine Thigh Infection and In Vitro Pharmacodynamic Models. *Antimicrob. Agents Chemother.* **2008**, *52* (6), 2156. (c) Sabath, L. D.; Garner, C.; Wilcox, C.; Finland, M. Susceptibility of Staphylococcus aureus and Staphylococcus epidermidis to 65 Antibiotics. *Antimicrob. Agents Chemother.* **1976**, *9* (6), 962−969.
(28) Enne, V. I.; Livermore, D. M.; Stephens, P.; Hall, L. M. C. Persistence of sulphonamide resistance in Escherichia coli in the UK despite national prescribing restriction. *Lancet* **2001**, *357* (9265), 1325−1328.
(29) Achari, A.; Somers, D.; Champness, J. N.; Bryant, P. K.; Rosemond, J.; Stammers, D. K. Crystal structure of the anti-bacterial sulfonamide drug target dihydropteroate synthase. *Nat. Struct. Biol.* **1997**, *4*, 490.
(30) (a) Kinnunen, T.-J. J.; Haukka, M.; Nousiainen, M.; Patrikka, A.; Pakkanen, T. A. Electron withdrawing and electron donating effects of 4,4′-bipyridine substituents on ruthenium mono(bipyridine) complexes. *J. Chem. Soc., Dalton Trans.* **2001**, No. 18, 2649−2654. (b) Ding, X.; Tuikka, M. J.; Hirva, P.; Kukushkin, V. Y.; Novikov, A. S.; Haukka, M. Fine-tuning halogen bonding properties of diiodine through halogen-halogen charge transfer - extended [Ru(2,2′-bipyridine)$(CO)_2X_2$]·I_2 systems (X = Cl, Br, I). *CrystEngComm* **2016**, *18* (11), 1987−1995.
(31) Mulhern, D.; Lan, Y.; Brooker, S.; Gallagher, J. F.; Görls, H.; Rau, S.; Vos, J. G. Synthesis and characterisation of a series of mononuclear ruthenium(II) carbonyl complexes of heterocycle-based asymmetric bidentate ligands. *Inorg. Chim. Acta* **2006**, *359* (3), 736−744.
(32) Rowland, R. S.; Taylor, R. Intermolecular Nonbonded Contact Distances in Organic Crystal Structures: Comparison with Distances Expected from van der Waals Radii. *J. Phys. Chem.* **1996**, *100* (18), 7384−7391.
(33) Knoll, J. D.; Albani, B. A.; Turro, C. New Ru(II) Complexes for Dual Photoreactivity: Ligand Exchange and 1O2 Generation. *Acc. Chem. Res.* **2015**, *48* (8), 2280−2287.
(34) Li, A.; Turro, C.; Kodanko, J. J. Ru(II) Polypyridyl Complexes Derived from Tetradentate Ancillary Ligands for Effective Photocaging. *Acc. Chem. Res.* **2018**, *51* (6), 1415−1421.
(35) Albada, H. B.; Chiriac, A.-I.; Wenzel, M.; Penkova, M.; Bandow, J. E.; Sahl, H.-G.; Metzler-Nolte, N. Modulating the activity of short arginine-tryptophan containing antibacterial peptides with N-terminal metallocenoyl groups. *Beilstein J. Org. Chem.* **2012**, *8*, 1753−1764.
(36) (a) Howe, R. A.; Spencer, R. C. Cotrimoxazole - Rationale for Re-Examining its Indications for Use. *Drug Saf.* **1996**, *14* (4), 213−218. (b) Masters, P. A.; O'Bryan, T. A.; Zurlo, J.; Miller, D. Q.; Joshi, N. Trimethoprim-Sulfamethoxazole Revisited. *Arch. Intern. Med.* **2003**, *163* (4), 402−410.
(37) Anderson, P. A.; Deacon, G. B.; Haarmann, K. H.; Keene, F. R.; Meyer, T. J.; Reitsma, D. A.; Skelton, B. W.; Strouse, G. F.; Thomas, N. C. Designed Synthesis of Mononuclear Tris(heteroleptic) Ruthenium Complexes Containing Bidentate Polypyridyl Ligands. *Inorg. Chem.* **1995**, *34* (24), 6145−6157.
(38) (a) Sheldrick, G. A short history of SHELX. *Acta Crystallogr., Sect. A: Found. Crystallogr.* **2008**, *64* (1), 112−122. (b) Sheldrick, G. Crystal structure refinement with SHELXL. *Acta Crystallographica Section C* **2015**, *71* (1), 3−8.
(39) Dolomanov, O. V.; Bourhis, L. J.; Gildea, R. J.; Howard, J. A. K.; Puschmann, H. OLEX2: a complete structure solution, refinement and analysis program. *J. Appl. Crystallogr.* **2009**, *42* (2), 339−341.

DOI: 10.1021/acs.inorgchem.9b01186
Inorg. Chem. XXXX, XXX, XXX−XXX